Absolute crystallinity and photocatalytic activity of brookite TiO$_2$ samples

Marianna Bellardita [a,*], Agatino Di Paola [a], Bartolomeo Megna [b], Leonardo Palmisano [a]

[a] "Schiavello-Grillone" Photocatalysis Group, Dipartimento di Energia, Ingegneria dell'informazione, e modelli Matematici (DEIM), University of Palermo, Viale delle Scienze, 90128 Palermo, Italy
[b] Dipartimento di Ingegneria Civile, Ambientale, Aerospaziale, dei Materiali (DICAM), University of Palermo, Viale delle Scienze, 90128 Palermo, Italy

ABSTRACT

This study reports a method to determine the absolute crystallinity of partly crystalline brookite TiO$_2$ photocatalysts. A natural, a commercial and various home-prepared brookite powders were characterized by X-ray diffraction analysis, Raman spectroscopy, scanning electron microscopy, UV–vis diffuse reflectance spectroscopy and nitrogen adsorption measurements. The absolute crystallinity was calculated from the ratio between the full width at half maximum intensity of the (121) X-ray diffraction peaks of the brookite samples and the (111) peak of CaF$_2$ as internal standard. The photocatalytic activity of the powders was tested employing the photodegradation of 4-nitrophenol as well as the selective oxidation of 4-methoxybenzyl alcohol to 4-methoxybenzaldehyde (*p*-anisaldehyde) under UV irradiation. The results indicated that crystallinity positively influenced the photooxidation of 4-nitrophenol and 4-methoxybenzyl alcohol but reduced the selectivity toward the synthesis of *p*-anisaldehyde.

© 2016 Elsevier B.V. All rights reserved.

1. Introduction

Titanium dioxide (TiO$_2$) is the most studied photocatalyst because of its high efficiency, non-toxicity, chemical and biological stability, and low cost. TiO$_2$ exists mainly in three different crystalline habits: rutile (tetragonal), anatase (tetragonal) and brookite (orthorombic). Pure brookite is rather difficult to be prepared so that its photocatalytic properties have been not much studied. Anatase is generally accepted to be a photocatalyst more efficient than rutile and brookite but recently, brookite has showed to be an interesting candidate for photocatalytic applications [1–13].

The photocatalytic activity of a TiO$_2$ powder depends on its physical properties such as crystal structure, degree of crystallinity, surface area, particle size and shape, surface hydroxyls content, etc. Brookite is composed of octahedra, each with a titanium atom at its center and oxygen atoms at its corners. The octahedra share edges and corners with each other to such an extent as to give the crystal the correct chemical composition [14]. Band gap energies ranging from 3.1 to 3.4 eV have been reported for brookite [1]. These values depended on the method of preparation and on the content of amorphous phase present in the samples.

The physical properties of brookite can be changed by calcination at different temperatures [2,5–8]. Thermal treatment increases crystallite size and crystallinity of the pristine sample [3,8,15] and decreases the surface area and the surface hydroxylation degree. Each of these parameters affects in different way the photocatalytic activity [16].

The presence of amorphous phase in TiO$_2$ samples is commonly considered to have no influence on the photocatalytic activity. This assumption, acceptable when the amount of amorphous phase is low, can be erroneous if its content becomes important. Ohtani et al. [17] showed that amorphous titania exhibits negligible reactivity in several photocatalytic reactions due to the facilitated recombination of electrons and holes at the traps on the surface and in the bulk of the particles. The increase of crystallinity leads to the reduction of crystal defects of the structure improving the separation rate of the photoinduced e$^-$/h$^+$ pairs.

Crystallite size and crystallinity can be evaluated by X-ray diffraction analysis. Inagaki et al. [18–20] qualitatively estimated the crystallinity of anatase powders by the full width at half maximum (FWHM) intensity of the 101 diffraction line of the X-ray powder patterns. To the best of our knowledge, only few papers have reported a quantitative analysis of the crystallinity of TiO$_2$ powders [21–25]. Ohtani et al. [17] evaluated the weight fraction of crystalline anatase in amorphous-anatase mixtures by means of differential scanning calorimetry (DSC) and powder X-ray diffraction (XRD) measurements. Jensen et al. [21–23] determined the

absolute crystallinity of anatase and rutile for different TiO$_2$ photocatalysts by X-ray diffraction analysis. No determination of the absolute crystallinity of brookite samples has ever been published.

The aim of this work was to determine the absolute crystallinity of brookite TiO$_2$ powders and to study the correlation between the photocatalytic activity of the samples and several properties, including crystallinity degree, surface area and particle size. The influence of the calcination temperature was also investigated. The samples were characterized by X-ray diffraction (XRD) analysis, scanning electron microscopy (SEM), diffuse reflectance spectroscopy (DRS), and BET specific surface area measurements. The photocatalytic activity was determined using the degradation of 4-nitrophenol (4-NP) and the selective oxidation of 4-methoxybenzyl alcohol (4-MBA) to 4-methoxybenzaldehyde (*p*-anisaldehyde, PAA) under UV light irradiation. The absolute crystallinity of the samples was determined by the XRD patterns using a simple quantitative method that can be used for partly crystalline brookite photocatalysts.

2. Experimental

2.1. Materials and instruments

Natural brookite used in this work was obtained from crystals collected from the Magnet Cove Complex, Arkansas (USA). The Cove is a 100-million-year old intrusive igneous body created by mantle-derived magma that pierced through existing Paleozoic sedimentary rocks. The average composition of the material was: Ti (0.965), Nb (0.017), V (0.008), Fe (0.008), Si (0.001) and Mg (0.001) [26]. The brookite crystals were black, due to interdispersed niobium practically impossible to be physically separated. Commercial brookite (99.99%) was supplied by Sigma as a flocculent white powder. Home-made brookite powder was obtained as follows: 10 mL of TiCl$_4$ were added dropwise to a solution containing 420 mL of water and 160 mL of concentrated hydrochloric acid at room temperature under stirring. Then the solution was heated in a closed bottle and aged for 48 h in an oven at 100 °C. The resultant precipitate contained a brookite–rutile mixture. Pure brookite was separated by peptization through several cycles of supernatant removal followed by water addition up to the initial volume. After a few washings, a dispersion of brookite particles formed, while the rutile phase remained as precipitate and it could thus be separated [27]. After removing the supernatant liquid, the obtained powders were collected and dried in vacuo at 55 °C. The home-made sample is referred as HP 100 °C.

X-ray diffraction patterns of the powders were recorded at room temperature on a PANalytical Empyrean diffractometer equipped with a PIXcel^{1D} (tm) detector using the CuKα radiation and a 2θ scan rate of 1.28 min^{-1}. The crystallite size of the samples was calculated by using the Scherrer equation. Raman spectra were obtained by means of a BWTek-i-micro Raman Plus System, equipped with a 785 nm diode laser. The power of the laser was 15% of the maximum value that was about 300 mW. The measurements were performed focusing the sample by a 20× magnification lens with a spot size of about 50 mm. The accuracy of the Raman shift was approximately 3 cm^{-1}. Scanning electron microscopy (SEM) observations were obtained using a FEI Quanta 200 ESEM microscope, operating at 20 kV on specimens upon which a thin layer of gold was deposited. An electron microprobe used in an energy dispersive mode (EDX) was employed to obtain information on the actual content of elements present in the samples.

The specific surface areas were determined with a Micromeritics ASAP^{TM} 2020 apparatus by using the five-points BET method. Pore volume and pore area distributions were obtained by the BJH method from the nitrogen adsorption-desorption isotherms at the liquid nitrogen temperature. Visible-ultraviolet spectra were recorded by diffuse reflectance spectroscopy in the range 200–800 nm by using a Shimadzu UV-2401 PC instrument with BaSO$_4$ as the reference sample. Photoluminescence (PL) spectra were recorded at room temperature with a Perkin Elmer LS45 Luminescence Spectrometry by exciting the samples at 320 nm.

The point of zero charge (pzc) of the samples was determined by the method of mass titration, which involves finding the asymptotic value of the pH of an oxide/water slurry as the oxide mass content is increased [28]. Thermogravimetric analysis was performed in the 30–750 °C range by means of a Netzsch Simultaneous Thermal Analyzer STA 449 Jupiter F1 with a nitrogen flux of ca. 20 mL min^{-1}, using alumina crucibles. The temperature program consisted of three steps: heating from 30 to 120 °C at 10 °C min^{-1}, isothermal step at 120 °C for 15 min, heating from 120 to 750 °C at 10 °C min^{-1}.

2.2. Photoreactivity experiments

2.2.1. 4-Nitrophenol degradation

A 0.5 L Pyrex batch reactor of cylindrical shape was used. In a typical experiment, 0.6 mg mL^{-1} of catalyst were suspended in an aqueous solution containing 20 mg L^{-1} of 4-nitrophenol (4-NP). The light source was a 125 W medium pressure Hg lamp (Helios Italquartz, Italy) with a maximum emission at about 365 nm, axially positioned within the photoreactor. The temperature of the suspension was controlled by circulation of water through a Pyrex thimble surrounding the lamp. The photon flux emitted by the lamp was $\Phi_i = 11$ mW cm^{-2}. O$_2$ was continuously bubbled for ca. 0.5 h before switching on the lamp and throughout the occurrence of the photoreactivity experiments. The temperature inside the reactor was ca. 30 °C. Samples of 5 mL were withdrawn at fixed intervals of time with a syringe, and the catalyst was separated from the solution by filtration through 0.2 μm Teflon membranes (Whatman). The quantitative determination of 4-nitrophenol was performed by measuring its absorption at 315 nm.

2.2.2. 4-Methoxybenzyl alcohol oxidation

The experiments were carried out in a cylindrical photoreactor (CPR, internal diameter: 32 mm and height: 188 mm) containing 150 mL of a suspension obtained adding 90 mg of catalyst to an aqueous solution of 4-methoxybenzyl alcohol at natural pH. The initial 4-MBA concentration was 0.5 mM. The reactor was irradiated by three external Actinic BL TL MINI 15 W/10 Philips fluorescent lamps whose main emission peak was in the near-UV region at 365 nm. The radiation intensity impinging on the suspension was measured by a radiometer Delta Ohm DO9721 with a UVA probe; the radiation power absorbed per unit volume of the suspension was about 0.76 mW mL^{-1}. The runs were carried out by using atmospheric air as oxidant agent and the lamps were switched on at time t = 0, after 0.5 h from the starting of the aeration. The temperature inside the reactor was ca. 30 °C. The values of substrate concentration before the addition of catalyst and before starting the irradiation were measured in order to determine the substrate adsorption on the catalyst surface under dark conditions. During the photoreactivity runs samples were withdrawn at fixed times and immediately filtered through 0.2 μm membranes (HA, Millipore) before analyses. The quantitative determination and identification of the starting molecules and their oxidation products were performed by means of a Beckman Coulter HPLC (System Gold 126 Solvent Module and 168 Diode Array Detector), equipped with a Phenomenex Kinetex 5 mm C18 100A column (4.6 mm × 150 mm) working at room temperature. The eluent consisted of a mixture of acetonitrile and 1 mM trifluoroacetic acid aqueous solution (20:80 volumetric ratio) and the flow rate was 0.8 mL min^{-1}. Retention times and UV spectra of the compounds
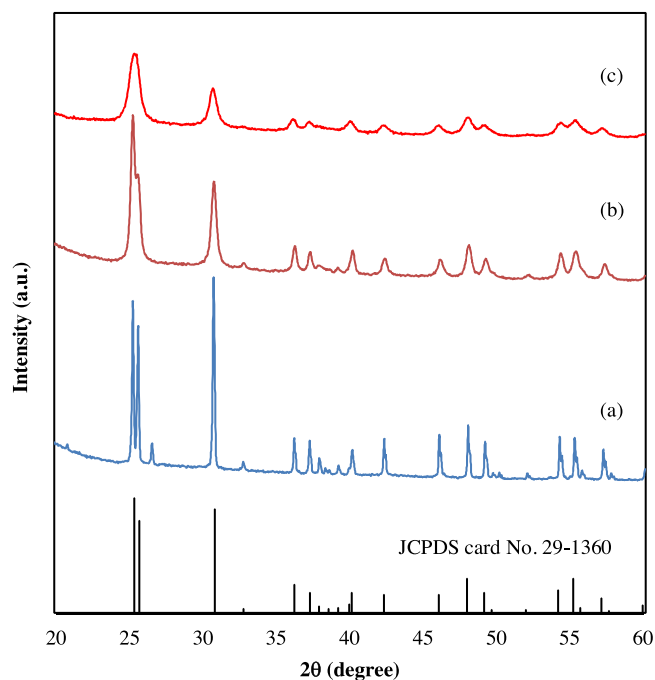
Fig. 1. XRD patterns of: (a) natural brookite, (b) commercial brookite, (c) HP brookite.

Fig. 2. Raman spectra of: (a) natural brookite, (b) commercial brookite, (c) HP brookite.

Fig. 3. UV–vis absorption spectra of: (a) commercial brookite, (b) HP brookite, (c) natural brookite.

were compared with those of standards. Standards of 4-MBA and PAA with a purity >99% were purchased from Sigma–Aldrich.

3. Results and discussion

3.1. Catalysts characterization

Fig. 1 shows the X-ray diffraction patterns of the natural, commercial and home-prepared brookite samples. The diffraction data of natural brookite (Fig. 1a) exactly corresponded to those reported in the JCPDS card No. 29–1360, that were obtained by using a specimen of Magnet Cove material. In particular, the diffractogram showed two separate main peaks at $2\theta = 25.40°$ and $25.72°$, respectively, and a third main peak at $2\theta = 30.81°$. All peaks are attributed to brookite with the exception of a small peak at $2\theta = 26.83°$, attributable to quartz. The peaks were very sharp and intense, indicating that the natural brookite sample was very crystalline. Differently, the peaks of commercial brookite (Fig. 1b) were quite broad and the peak at $2\theta = 25.34°$ overlapped with the peak at $25.69°$. The broad features exhibited by the diffractogram of the home-prepared sample (Fig. 1c) indicated a poorly crystallized brookite phase.

Fig. 2 shows the Raman spectra of the three samples. The Raman peaks were in good agreement with the mode frequencies predicted by density function theory (DFT) calculations of lattice dynamics [29], confirming that the samples were single-phase brookite. The lattice of brookite has a D_{2h}^{15} (*Pbca*) symmetry [30] and according to the group theory, there are 36 Raman active optical modes ($9 A_{1g} + 9 B_{1g} + 9 B_{2g} + 9 B_{3g}$) in the range from 100 to $700 \, cm^{-1}$. The spectrum of commercial brookite showed 15 peaks including six A_{1g} (128, 153, 195, 245, 413, 637 cm^{-1}), three B_{1g} (214, 287, 322 cm^{-1}), four B_{2g} (367, 397, 462, 585 cm^{-1}) and two B_{3g} (502, 545 cm^{-1}) modes [29,31]. Two peaks at 287 and 397 cm^{-1} were not present in the spectrum of the home-prepared brookite sample whilst only 8 peaks were detected in the spectrum of the natural sample. Unexpectedly, the high crystallinity inferred from the XRD pattern of the natural sample was not verified by the small and diffuse peaks of the Raman spectrum probably because the
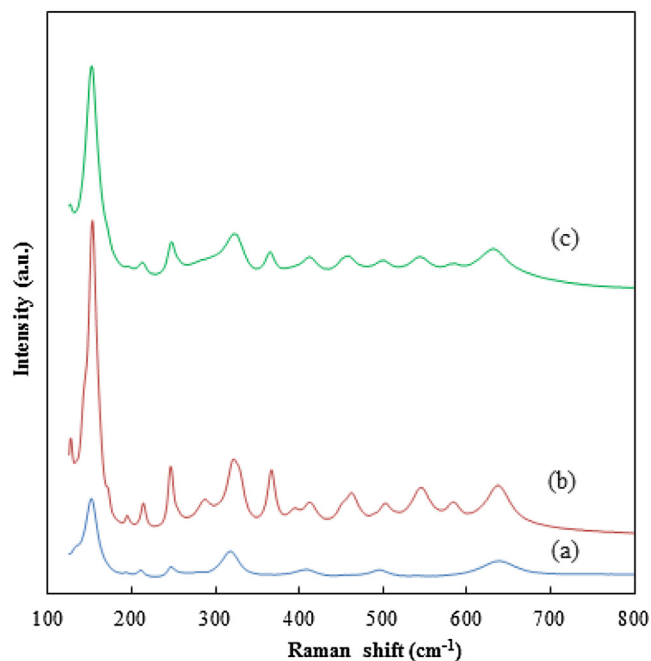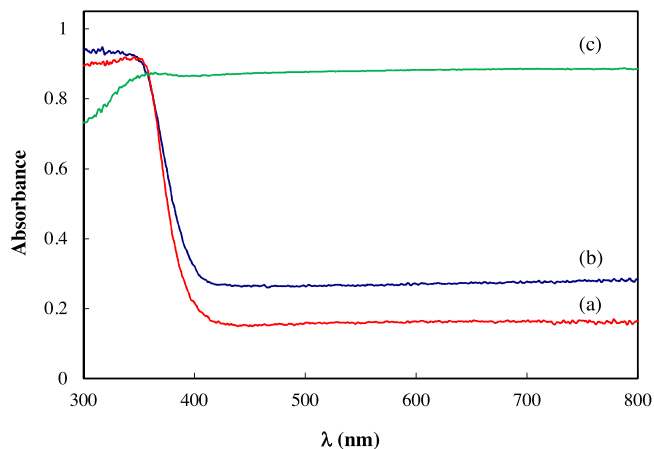
Raman scattering efficiency as well as the relative band intensities depend on many sample features apart from the crystal phase, such as nanocrystal size, shape and surface status [32].

Fig. 3 shows the UV–vis absorption spectra of the three samples. The spectra of the white commercial and home-prepared samples were similar whilst that of natural brookite was completely different. In particular, the natural sample strongly absorbed in the visible region since the crystals from the Magnet Cove complex were black due to the small amount of interspersed niobium [26]. The band gap values (E_g) of the commercial and home-prepared brookite samples were estimated by extrapolation of the linear part of the plots of $(\alpha h\nu)^2$ versus the energy of the exciting light [33] assuming that brookite was an indirect semiconductor [4,34]. As shown in Table 1, the E_g values resulted 3.27 and 3.22 eV, respectively. The small differences between the band gap values of the two samples were probably related to their different degrees of crystallization. The band gap of the natural sample was not determined due to the atypical spectrum of the black crystals

Table 1
Characteristics of the various brookite samples.

Sample	Crystallinity (%)	Specific surface area ($m^2\,g^{-1}$)	Band gap energy (eV)	Crystallite size (nm)	Pore volume ($cm^3\,g^{-1}$)	Pore diameter (nm)
HP 100 °C	26.6	100	3.22	14.6	0.30	14.2
HP 300 °C	28. 6	66	3.24	16.1	0.34	20.1
HP 450 °C	40.4	40	3.27	23.4	0.29	29.6
HP 600 °C	43.7	37	3.27	26.5	0.32	35.3
HP 700 °C	56.5	26	3.29	40.4	0.27	42.4
commercial	39.4	37	3.27	22.6	0.36	40.0
natural	100.0	<1	–	–		

Note: the crystallite size of the natural sample is not reported because the Scherrer equation is not applicable to crystals larger than 100 nm.
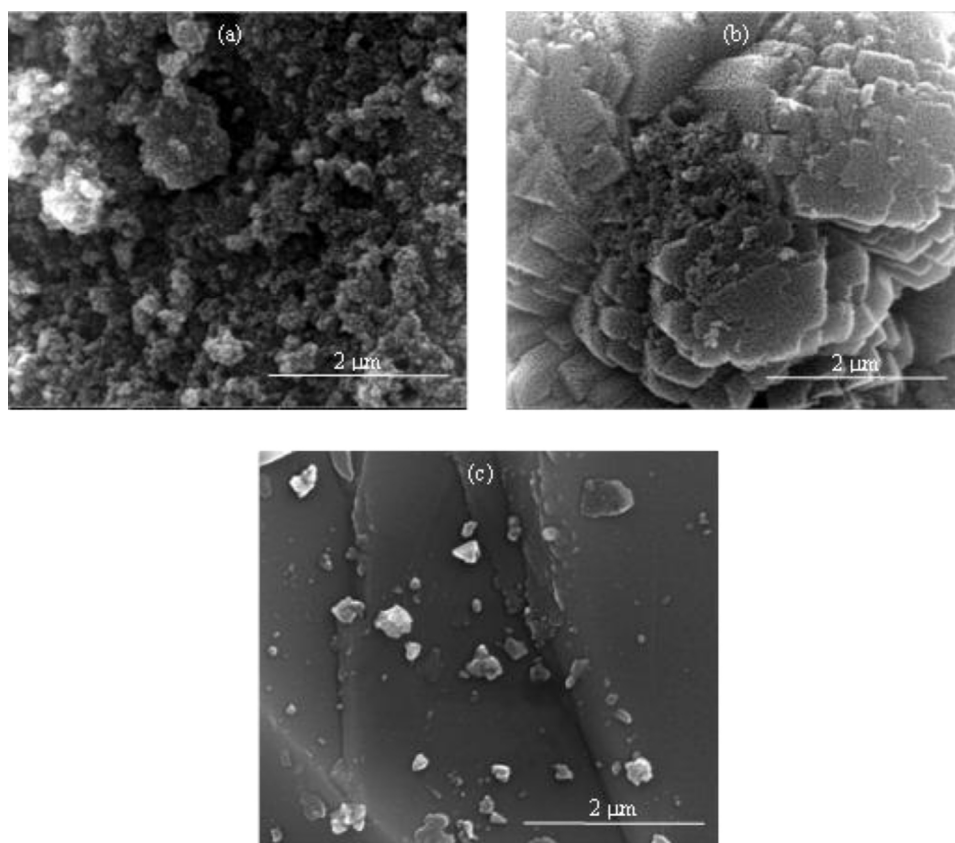

Fig. 4. SEM micrographs of: (a) HP brookite (b) commercial brookite, (c) natural brookite.

SEM observations revealed that the three samples exhibited quite different morphologies. The home-prepared sample consisted of small particles agglomerated into larger clusters with rough surfaces (Fig. 4a) whereas the commercial sample showed a terraced flower-like structure (Fig. 4b). The average sizes of the primary particles were quite close to those calculated from the XRD patterns. Differently, the micrograph of natural brookite (Fig. 4c) evidenced a great number of smooth particles with variable sizes and geometries depending on the grinding of the big original crystals.

Fig. 5 shows the N_2 adsorption-desorption isotherms of the three brookite samples. The commercial and home-prepared samples exhibited Type IV isotherms [35] which are associated with capillary condensation taking place in mesopores. The hysteresis loop exhibited by the commercial sample showed two branches almost vertical and nearly parallel over an appreciable range of gas uptake which are typical of H1 hysteresis whereas the loop of the

home-prepared sample is attributable to a H2 type hysteresis. The isotherms of the natural sample were practically flat without hysteresis in agreement with the non porous structure of the mineral brookite crystals as evidenced by the SEM micrographs.

The specific surface areas of the three samples were calculated from the corresponding isotherms and are reported in Table 1. The specific surface area of the commercial sample ($37\,m^2\,g^{-1}$) was lower than that of the home-prepared brookite ($100\,m^2\,g^{-1}$), indicating a higher particle agglomeration. The surface area of the crystalline natural sample was very low ($<1\,m^2\,g^{-1}$).

Table 1 also reports characteristics of the powders obtained by calcination of the home-prepared sample at 300, 450, 600 and 700 °C for 2 h, referred to as HP 300 °C, HP 450 °C, HP 600 °C, and HP 700 °C, respectively.

Fig. 6 shows the XRD patterns of the samples calcined at the various temperatures. The intensity of the brookite peaks increased with increasing temperature and no change of the crystal struc-
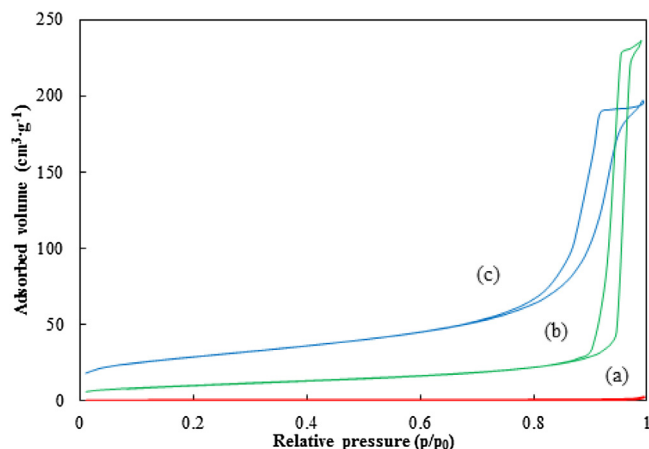
Fig. 5. N$_2$ adsorption-desorption isotherms of: (a) natural brookite, (b) commercial brookite, (c) HP brookite.
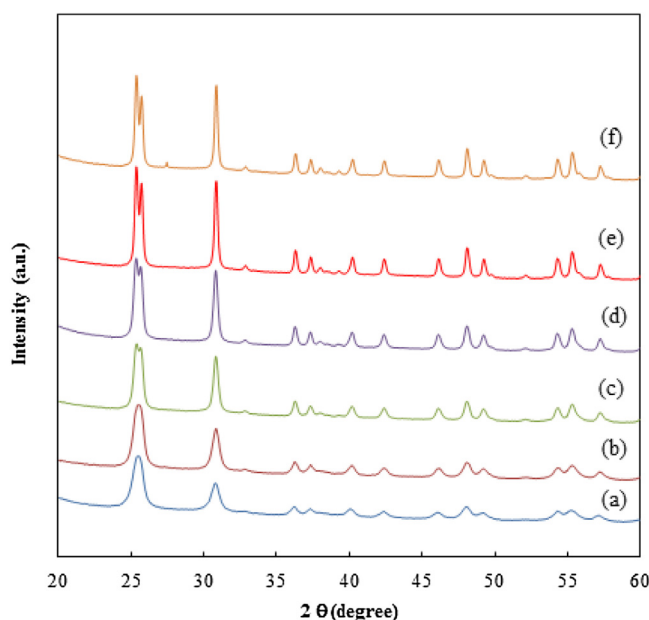

Fig. 6. XRD patterns of the samples obtained by calcination of HP 100 °C at different temperatures for 2 h: (a) as-prepared, (b) 300 °C, (c) 450 °C, (d) 600 °C, (e) 700 °C, (f) 750 °C.

ture was observed up to 700 °C. A small peak of rutile appeared in the diffractogram recorded at 750 °C. The increase of peak intensities with temperature is attributable to the crystallization of amorphous TiO$_2$ to brookite crystallites. In agreement with previous works [5,27,36], the transformation brookite → rutile occurred without the involvement of the anatase polymorph.

The average particle sizes of the brookite samples were determined by applying the Sherrer equation to the (121) diffraction peaks. As shown in Table 1, the crystallite size increased with increasing temperature whereas the SSA decreased progressively. All calcined samples showed type IV isotherms with hysteresis loops of type H2. With increasing temperature, the loops shifted to the region of higher relative pressure and the areas of the hysteresis loops gradually became small. The average pore size of the samples increased from 14.2 to 42.4 nm due to the sintering and crystal growth of the brookite particles. Differently, the pore volume changes were random. The small increase of band gap values exhibited by the samples with increasing calcination temperature is attributable to the gradual increasing of the crystallinity of the solids.

3.2. Absolute crystallinity

The differences of crystallinity among the brookite samples can be roughly evaluated by the relative intensities of the strongest XRD peaks, but the real fraction of crystalline and amorphous phases is difficult to be determined. Jensen et al. [21] calculated the absolute crystallinity of partly crystalline TiO$_2$ photocatalysts with respect to a 100% crystalline CaF$_2$ sample. The areas of the 100% peak of anatase (101) and the 100% peak of CaF$_2$ (220) were determined from the XRD patterns and the value obtained from the ratio between the area of the unknown anatase sample and that of CaF$_2$ to 1.25 was used to obtain the absolute crystallinity of the TiO$_2$ sample. The value of 1.25 used for anatase was obtained from the ratio between the area of 100% crystalline anatase (101) peak and that of CaF$_2$ (220) in a 50% weight ratio. The corresponding ratio between crystalline rutile (110) and CaF$_2$ (220) was 0.90.

The method proposed by Jensen et al. [21] could be employed for brookite samples but, unlikely, no ratio between 100% crystalline brookite and CaF$_2$ is reported in literature probably because of the difficulty to have a 100% brookite sample. The availability of the Magnet Cove brookite crystals seemed a good opportunity to obtain the ratio between brookite and CaF$_2$ but unexpected drawbacks prevented the calculation of this value.

As reported in the diffraction data file [JCPDS 29-1360], the XRD pattern of brookite is characterized by three main peaks: (120) at $2\theta = 25.34°$, (111) at $2\theta = 25.69°$ and (121) at $2\theta = 30.81°$. The former peak is the most intense ($I^{(120)} = 100$) but overlaps with the (111) peak ($I^{(111)} = 80$), so that a correct evaluation of its area is practically impossible, especially in poorly crystalline samples.

This difficulty could be overcome by comparing the total area of the two peaks with the area of the (220) peak of CaF$_2$. Another possibility could be to choose the area of the (121) peak ($I^{(121)} = 90$) for the comparison with that of CaF$_2$ (220). Anyway, the areas of the main peaks exhibited by the diffractogram of the Magnet Cove crystals were lower than those of the less crystalline commercial and home-prepared (HP) brookite samples (Fig. 1) and consequently, the estimation of the percentages of the crystalline and amorphous phases was meaningless.

Inagaki et al. [18–20] found a correlation between the crystallinity of anatase powders and the full width at half maximum of X-ray diffraction lines. A quantitative estimation of the crystallinity of partly crystalline brookite samples can then be obtained by using the FWHM of the (121) peak rather than the area as suggested by Jensen et al. [21].

The crystallinity of the brookite samples was evaluated with reference to 100% crystalline CaF$_2$, used as internal standard. The samples were mixed with CaF$_2$ (50 wt%) and the XRD patterns were recorded. The ratio between the FWHM value of the (111) peak of CaF$_2$ and the FWHM value of the (121) peak of the (100%) crystalline natural sample was taken as the reference. The measurements were repeated twice (the accuracy of the measure was verified by the constancy of the FWHM values for the two samples) and the following value was obtained:

$$\frac{\text{FWHM}_{\text{CaF}_2,111}}{\text{FWHM}_{\text{brookite},121}} = \frac{0.161}{0.154} = 1.04 \tag{1}$$

In order to reduce the influence of the incident angle of the divergent X-ray beam, the (111) peak of CaF$_2$ was selected as reference rather than the (220) peak since the former is near to the (121) peak of brookite used to calculate the ratio of the FWHM values

Fig. 7 shows the XRD patterns of the mixtures obtained by mixing CaF$_2$ and the samples obtained by calcination of HP 100 °C at different temperatures. The values of FWHM continuously decreased with increasing the temperature confirming the enhancement of the crystallinity of the samples. By comparing the values obtained from the ratios between the FWHM values of the
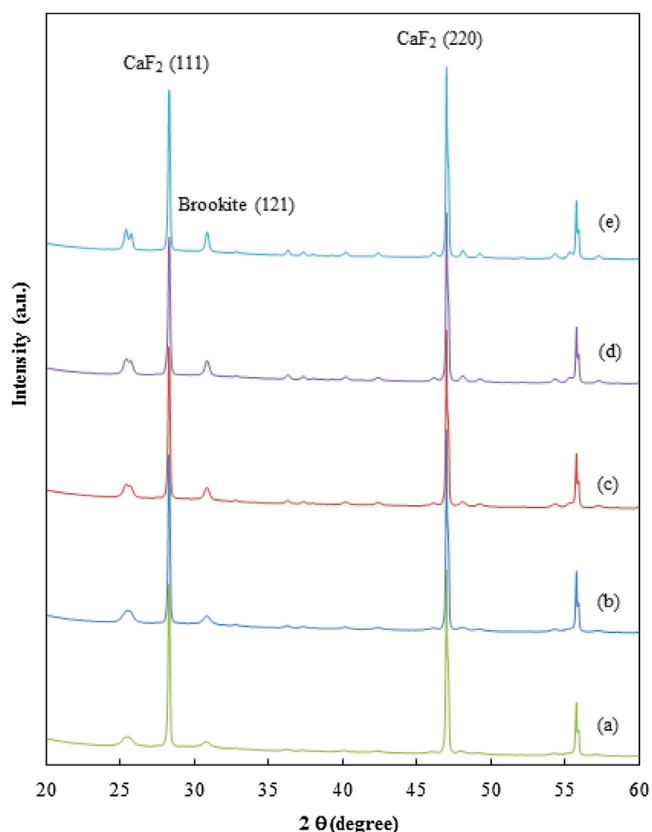
Fig. 7. XRD patterns of the HP brookite samples mixed with CaF$_2$ in a 50% wt ratio: (a) HP 100 °C, (b) HP 300 °C, (c) HP 450 °C, (d) HP 600 °C, (e) HP 700 °C.

Table 2
Photoreactivity assessment of the brookite samples via 4-NP degradation or 4-MBA oxidation.

Sample	4-NP	4-MBA		
	$r_o \times 10^{9a}$ (mol L^{-1} s^{-1})	$r_o \times 10^{9b}$ (mol L^{-1} s^{-1})	X^c (%)	S^c (%)
HP 100 °C	8.5	6.0	19.7	57.1
HP 300 °C	7.1	5.2	17.5	66.0
HP 450 °C	12.9	10.7	26.5	53.4
HP 600 °C	12.5	9.8	26.3	56.1
HP 700 °C	15.4	12.2	29.2	42.8
commercial	29.1	28.5	43.9	31.7
natural	4.6	1.4	7.4	27.4

[a] Initial 4-NP photodegradation rate.
[b] Initial 4-MBA photodegradation rate.
[c] Conversion (X) of 4-MBA and selectivity (S) to PAA calculated after 4 h of irradiation.
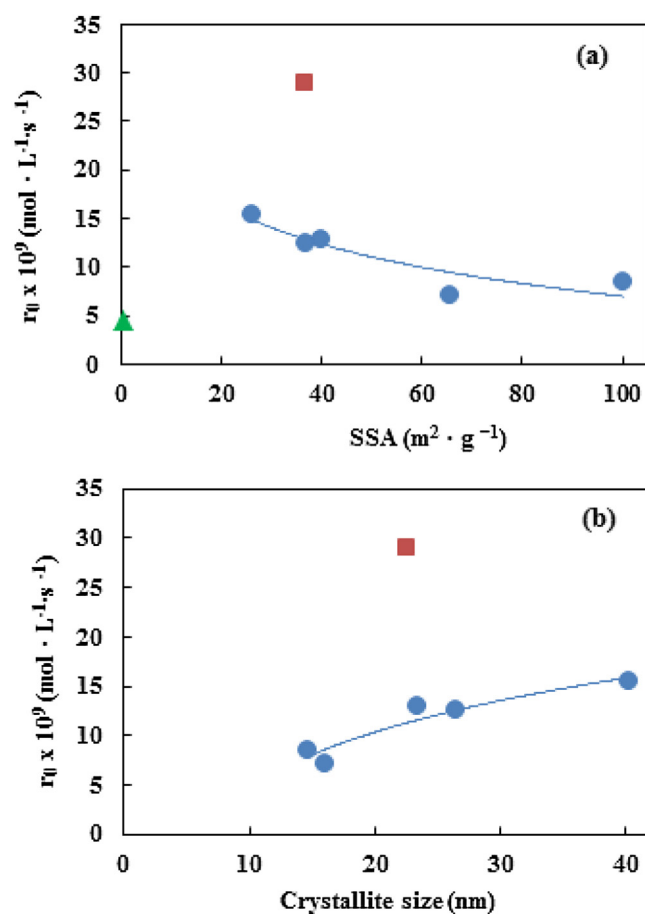

Fig. 8. Initial 4-NP photodegradation rate as a function of (a) specific surface area and (b) crystallite size of: (●) HP samples calcined at different temperatures, (■) commercial brookite, (▲) natural brookite. (For interpretation of the references to colour in this figure legend, the reader is referred to the web version of this article.)

(111) peak of CaF$_2$ and the (121) peak of the various samples to 1.04, it was possible to evaluate the absolute crystallinity of the brookite powders. In Table 1 are reported the values of the calculated crystallinity degree of the various samples. The HP 100 °C sample showed a low value of crystallinity (26.6%) that increased with the temperature reaching the maximum amount of 56.5% by annealing at 700 °C. It was not possible to further enhance the crystallinity of the samples by increasing the temperature or the duration of the thermal treatment because brookite progressively transformed into rutile. The commercial sample was partly crystalline with a crystallinity percentage (39.4%) similar to that of the sample annealed at 450 °C.

3.3. Photocatalytic activity

The decomposition of 4-nitrophenol was followed by determining the concentration of the substrate at various time intervals. The degradation rate, r_0, was calculated from the initial slope of the concentration versus time profiles. The r_0 values are reported in Table 2.

All the powders were active for the photodegradation of the substrate although the efficiency of commercial brookite was 2–4 times higher than that of the home-made samples. The lowest photoactivity was exhibited by natural brookite.

As shown in Fig. 8, a good correlation was found between photoactivity and specific surface area or crystallite size of the samples calcined at different temperatures. In particular, the photoactivity decreased with increasing the surface area of the samples but increased with increasing the crystallite size. Similar results (not shown for the sake of brevity) were obtained for the degradation of 4-MBA.

Both crystallite size and specific surface area are related to the crystallinity of the samples. Fig. 9 shows the dependence of the r_0 values of the two different photocatalytic reactions on the percentages of crystallinity of the various samples. Calcination of the home-prepared (HP) sample improved the rate of decomposition of both substrates due to the increase of crystallinity caused by the heat treatment.

The photocatalytic oxidation of 4-methoxybenzyl alcohol in aqueous solution proceeds through two parallel reaction routes active from the start of irradiation: the first route is a partial oxidation producing p-anisaldehyde (PAA) and the second one is the mineralization of 4-methoxybenzyl alcohol to CO$_2$. The latter
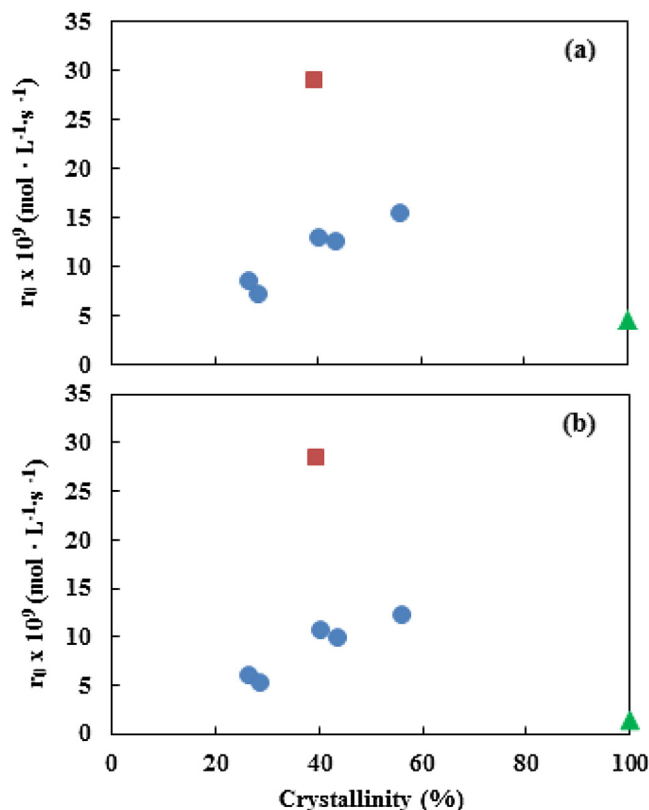
Fig. 9. Initial photodegradation rate of (a) 4-NP and (b) 4-MBA as a function of the crystallinity of: (●) HP samples calcined at different temperatures, (■) commercial brookite, (▲) natural brookite. (For interpretation of the references to colour in this figure legend, the reader is referred to the web version of this article.)

Fig. 10. (a) Conversion of 4-MBA and (b) selectivity to PAA after 4 h of irradiation as a function of the crystallinity of: (●) HP samples calcined at different temperatures, (■) commercial brookite, (▲) natural brookite. (For interpretation of the references to colour in this figure legend, the reader is referred to the web version of this article.)

occurs through a series of reactions taking place over the catalyst surface and producing intermediates which do not desorb into the bulk of the solution. The process performance was followed by measuring the values of alcohol and aldehyde concentration and calculating the substrate conversion and the selectivity toward the aldehyde. Table 2 reports the values of conversion of 4-MBA and selectivity to PAA determined after 4 h of irradiation of the various brookite samples.

As shown in Fig. 10a, the conversion of 4-MBA in the presence of commercial brookite was higher than that obtained by irradiation of the home-made samples. Once more, natural brookite was the least reactive among the tested photocatalysts.

The results indicate that the conversion of 4-MBA increased with increasing the crystallinity of the home-made samples whereas, at variance, the selectivity to *p*-anisaldehyde decreased. The most crystalline powders degraded both the substrate and its intermediates owing to their elevated oxidant power. The higher was the percentage of amorphous phase, the greater was the amount of defects and therefore the higher was the probability of entrapment of the hole–electron pairs, thus reducing the conversion of 4-MBA. Differently, the lowest reactivity of the least crystalline samples favoured the desorption of *p*-anisaldehyde that was not further on oxidized over the catalyst surface. The anti-correlation between oxidant power and selectivity was corroborated by the results obtained with the commercial sample that exhibited a value of photoactivity higher than that of the calcined samples but, conversely, a lower selectivity. The anomalous photocatalytic behaviour exhibited by the mineral sample is attributable to its particular characteristics as, for instance, very low specific surface area and non porous structure.
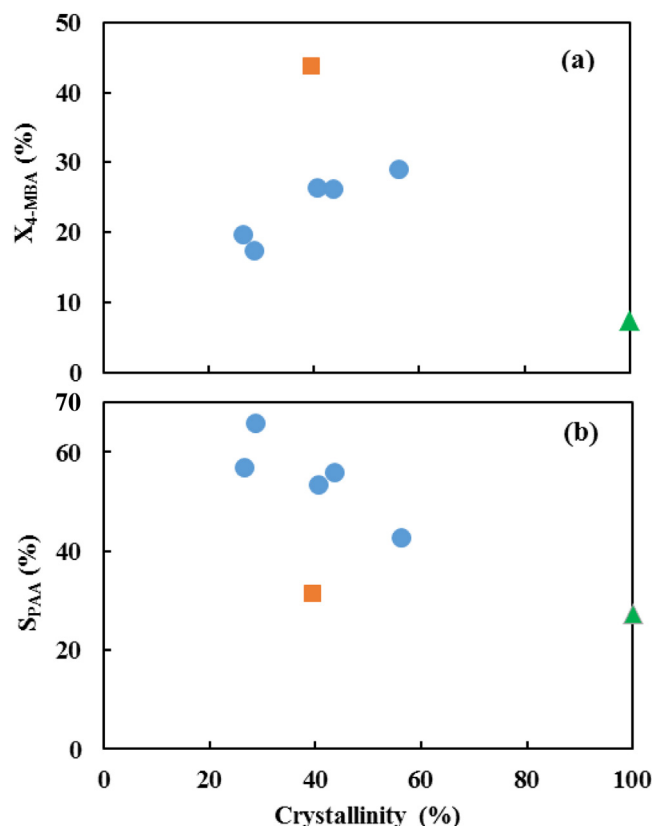
Notably, the photocatalytic performances of the commercial sample were somewhat different from those of the sample calcined at 450 °C although the values of many physical characteristics were quite comparable. In particular, crystallinity, specific surface area and crystal size were almost the same. On the other hand, it is known that the photoactivity of a catalyst depends on many physico-chemical parameters as for instance porosity, surface acidity, extent of surface hydroxylation, etc. Moreover, the intrinsic electronic properties are also paramountly important.

Fig. 11 shows the comparison between the N_2 adsorption-desorption isotherms of the two samples. The BJH pore size ranged from 5 to 50 nm for HP 450 °C and from 5 to 75 nm for the commercial sample. Generally, the presence of a porous structure is extremely useful in heterogeneous photocatalysis because it facilitates the access of the reactant molecule to the surface and favours the desorption of the products. The highest reactivity of commercial brookite with respect to the home-prepared sample could be related to the largest amount of substrate adsorbed in the dark (6.5 and 4.4 mol% of 4-NP and 4.3 and 1.5 mol% of 4-MBA, respectively) and/or to the differences of zero charge points (2.2 for the commercial sample and 3.4 for HP 450 °C).

As shown in Fig. 12, the thermogravimetric analysis of HP 450 °C revealed a continuous mass loss from 120 to 750 °C that can be related to weakly and strongly bonded OH groups. The total hydroxyl groups weight percentage corresponded to about 1%. Differently, a very low weight loss was measured for the commercial sample in the whole temperature range, indicating a scarce presence of hydroxyl groups on the surface. As reported in a previous work [37] there is a good correlation between the photocatalytic activity of TiO$_2$ powders and the percentages of surface OH groups. In particular, with increasing the amount of surface OH groups
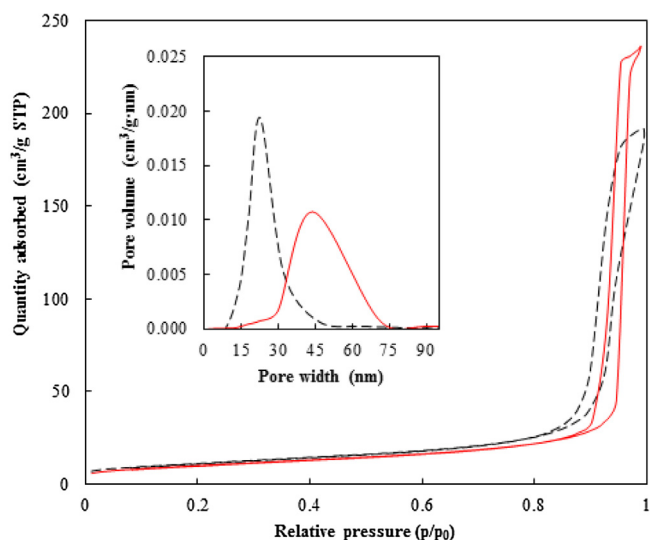
Fig. 11. N$_2$ adsorption-desorption isotherms: (full line) commercial brookite, (dashed line) HP 450 °C. Inset: pore size distribution.
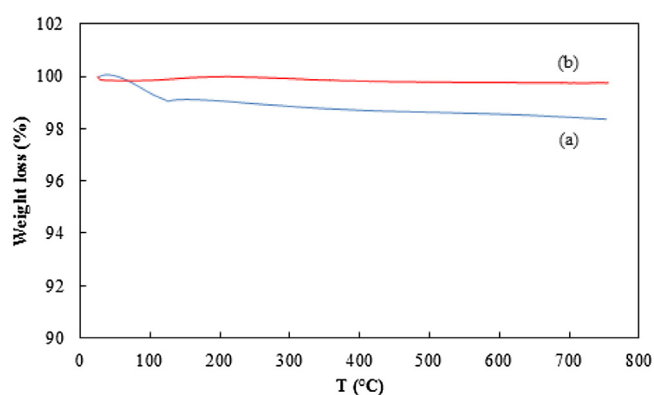

Fig. 12. Weight percentage losses as a function of temperature: (a) HP 450 °C, (b) commercial brookite.

Fig. 13. Room temperature photoluminescence spectra: (a) HP 450 °C, (b) commercial brookite. (λ_{exc} = 320 nm).

the photoactivity for the degradation of 4-nitrophenol decreased whereas the selectivity toward the oxidation of 4-methoxybenzyl alcohol to *p*-anisaldehyde increased.

Fig. 13 shows the photoluminescence spectra of the commercial and HP 450 °C samples. Although the shape of the spectra was very similar indicating the same electronic band structure, the commercial sample exhibited a stronger photoluminescence signal. The differences are due to a different content of defects and/or oxygen vacancies induced by different preparation methods.

The above characterization results are in agreement with the findings of Ohtani et al. [17] who reported that many anatase TiO$_2$ powders available commercially or prepared in laboratories showed extensively different photocatalytic activity. This means that the titanium precursor and the synthesis conditions influence the photoactivity.

4. Conclusions

The absolute crystallinity of partly crystalline brookite samples can be determined from the full width at half maximum intensity of the (121) X-ray diffraction peaks. The crystallinity degree of home-prepared samples calcined at different temperatures affects the photocatalytic activity for the 4-nitrophenol degradation and the selective oxidation of 4-methoxybenzyl alcohol to *p*-anisaldehyde. In particular, the most crystalline samples
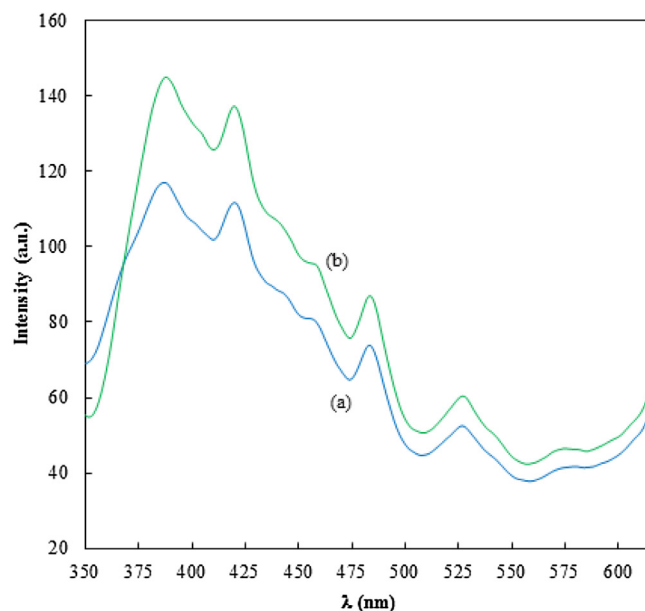
were the most efficient for the oxidation of 4-nitrophenol or 4-methoxybenzyl alcohol whereas the highest selectivity toward the synthesis of *p*-anisaldehyde was obtained in the presence of the least crystalline powders. These results demonstrated the importance of quantitative measurements of the crystallinity degree of the samples.

References

[1] A. Di Paola, M. Bellardita, L. Palmisano, Brookite, the least known TiO$_2$ photocatalyst, Catalysts 3 (2013) 36–73.
[2] H. Kominami, Y. Ishii, M. Kohno, S. Konishi, Y. Kera, B. Ohtani, Nanocrystalline brookite-type titanium(IV) oxide photocatalysts prepared by a solvothermal method: correlation between their physical properties and photocatalytic activities, Catal. Lett. 91 (2003) 41–47.
[3] J. Xie, X. Lü, J. Liu, H. Shu, Brookite titania photocatalytic nanomaterials: synthesis, properties, and applications, Pure Appl. Chem. 81 (2009) 2407–2415.
[4] T.A. Kandiel, A. Feldhoff, L. Robben, R. Dillert, D.W. Bahnemann, Tailored titanium dioxide nanomaterials: anatase nanoparticles and brookite nanorods as highly active photocatalysts, Chem. Mater. 22 (2010) 2050–2060.
[5] J.-G. Li, C. Tang, D. Li, H. Haneda, T. Ishigaki, Monodispersed spherical particles of brookite-type TiO$_2$: synthesis, characterization, and photocatalytic property, J. Am. Ceram. Soc. 87 (2004) 1358–1361.
[6] J. Zhang, S. Yan, L. Fu, F. Wang, M. Yuan, G. Luo, Q. Xu, X. Wang, C. Li, Photocatalytic degradation of rhodamine B on anatase, rutile, and brookite TiO$_2$, Chin. J. Catal. 32 (2011) 983–991.
[7] V. Štengl, D. Králová, Photoactivity of brookite–rutile TiO$_2$ nanocrystalline mixtures obtained by heat treatment of hydrothermally prepared brookite, Mater. Chem. Phys. 129 (2011) 794–801.
[8] Z. Li, S. Cong, Y. Xu, Brookite vs anatase TiO$_2$ in the photocatalytic activity for organic degradation in water, ACS Catal. 4 (2014) 3273–3280.
[9] M. Inada, K. Iwamoto, N. Enomoto, J. Hojo, Synthesis and photocatalytic activity of small brookite particles by self-hydrolysis of TiOCl$_2$, J. Ceram. Soc. Jpn. 119 (2011) 451–455.
[10] H. Lin, L. Li, M. Zhao, X. Huang, X. Chen, G. Li, R. Yu, Synthesis of high-quality brookite TiO$_2$ single-crystalline nanosheets with specific facets exposed: tuning catalysts from inert to highly reactive, J. Am. Chem. Soc. 134 (2012) 8328–8331.
[11] K.-I. Katsumata, Y. Ohno, K. Tomita, T. Taniguchi, N. Matsushita, K. Okada, Synthesis of amphiphilic brookite nanoparticles with high photocatalytic

performance for wide range of application, ACS Appl. Mater. Interfaces 4 (2012) 4846–4852.

[12] Y. Zou, X. Tan, T. Yu, Y. Li, Q. Shang, W. Wang, Synthesis and photocatalytic activity of chrysanthemum-like brookite TiO$_2$ nanostructures, Mater. Lett. 132 (2014) 182–185.

[13] M. Altomare, M.V. Dozzi, G.L. Chiarello, A. Di Paola, L. Palmisano, E. Selli, High activity of brookite TiO$_2$ nanoparticles in the photocatalytic abatement of ammonia in water, Catal. Today 252 (2015) 184–189.

[14] X. Bokhimi, A. Morales, M. Aguilar, J.A. Toledo-Antonio, F. Pedraza, Local order in titania polymorphs, Int. J. Hydrogen Energy 26 (2001) 1279–1287.

[15] S. Bakardjieva, V. Štengl, L. Szatmary, J. Šubrt, J. Lukac, D. Nižnanský, K. Čížek, J. Jirkovský, N. Petrova, Tranformation of brookite-type TiO$_2$ nanocrystals to rutile: correlation between microstructure and photoactivity, J. Mater. Chem. 16 (2006) 1709–1716.

[16] B. Ohtani, Preparing articles on photocatalysis—beyond the illusions, misconceptions, and speculation, Chem. Lett. 37 (2008) 217–229.

[17] B. Ohtani, Y. Ogawa, S.-I. Nishimoto, Photocatalytic activity of amorphous anatase mixture of titanium(IV) oxide particles suspended in aqueous solutions, J. Phys. Chem. B 101 (1997) 3746–3752.

[18] M. Toyoda, Y. Nanbu, Y. Nakazawa, M. Hirano, M. Inagaki, Effect of crystallinity of anatase on photoactivity for methyleneblue decomposition in water, Appl. Catal. B: Environ. 49 (2004) 227–232.

[19] M. Inagaki, T. Imai, T. Yoshikawa, B. Tryba, Photocatalytic activity of anatase powders for oxidation of methylene blue in water and diluted NO gas, Appl. Catal. B: Environ. 51 (2004) 247–254.

[20] M. Inagaki, R. Nonaka, B. Tryba, A.W. Morawski, Dependence of photocatalytic activity of anatase powders on their crystallinity, Chemosphere 64 (2006) 437–445.

[21] H. Jensen, K.D. Joensen, J.-E. Jørgensen, J.S. Pedersen, E.G. Søgaard, Characterization of nanosized partly crystalline photocatalysts, J. Nanopart. Res. 6 (2004) 519–526.

[22] H. Jensen, A. Soloviev, Z. Li, E.G. Søgaard, XPS and FTIR investigation of the surface properties of different prepared titania nano-powders, Appl. Surf. Sci. 246 (2005) 239–249.

[23] M.E. Simonsen, H. Jensen, Z. Li, E.G. Søgaard, Surface properties and photocatalytic activity of nanocrystalline titania films, J. Photochem. Photobiol. A: Chem. 200 (2008) 192–200.

[24] M. Bellardita, V. Augugliaro, V. Loddo, B. Megna, G. Palmisano, L. Palmisano, M.A. Puma, Selective oxidation of phenol and benzoic acid in water via home prepared TiO$_2$ photocatalysts: distribution of hydroxylation products, Appl. Catal. A: Gen. 441–442 (2012) 79–89.

[25] X. Wang, L. Sø, R. Su, S. Wendt, P. Hald, A. Mamakhel, C. Yang, Y. Huang, B.B. Iversen, F. Besenbacher, The influence of crystallite size and crystallinity of anatase nanoparticles on the photo-degradation of phenol, J. Catal. 310 (2014) 100–108.

[26] M.J.K. Flohr, Titanium vanadium and niobium mineralization and alkali metasomatism from the Magnet Cove Complex, Arkansas, Econ. Geol. 89 (1994) 105–130.

[27] A. Di Paola, G. Cufalo, M. Addamo, M. Bellardita, R. Campostrini, M. Ischia, R. Ceccato, L. Palmisano, Photocatalytic activity of nanocrystalline TiO$_2$ (brookite, rutile and brookite-based) powders prepared by thermohydrolysis of TiCl$_4$ in aqueous chloride solutions, Colloids Surf. A 317 (2008) 366–376.

[28] J.S. Noh, J.A. Schwarz, Estimation of the point of zero charge of simple oxides by mass titration, J. Colloid Interface Sci. 130 (1989) 157–164.

[29] M.N. Iliev, V.G. Hadjiev, A.P. Litvinchuk, Raman and infrared spectra of brookite (TiO$_2$): experiment and theory, Vib. Spectrosc. 64 (2013) 148–152.

[30] L. Pauling, J.H. Sturdivant, The crystal structure of brookite, Z. Kristall. 68 (1928) 239–256.

[31] G.A. Tompsett, G.A. Bowmaker, R.P. Cooney, J.B. Metson, K.A. Rodgers, J.M. Seakins, The Raman spectrum of brookite, TiO$_2$ (Pbca, Z = 8), J. Raman Spectrosc. 26 (1995) 57–62.

[32] R. Buonsanti, V. Grillo, E. Carlino, C. Giannini, T. Kipp, R. Cingolani, P.D. Cozzoli, Nonhydrolytic synthesis of high-quality anisotropically shaped brookite TiO$_2$ nanocrystals, J. Am. Chem. Soc. 130 (2008) 11223–11233.

[33] Y.I. Kim, S.J. Atherton, E.S. Brigham, T.E. Mallouk, Sensitized layered metal oxide semiconductor particles for photochemical hydrogen evolution from nonsacrificial electron donors, J. Phys. Chem. 97 (1993) 11802–11810.

[34] M. Koelsch, S. Cassaignon, J.F. Guillemoles, J.P. Jolivet, Comparison of optical and electrochemical properties of anatase and brookite TiO$_2$ synthesized by the sol–gel method, Thin Solid Films 403–404 (2002) 312–319.

[35] K.S.W. Sing, D.H. Everett, R.A.W. Haul, L. Moscou, R.A. Pierotti, J. Rouquérol, T. Siemieniewska, Reporting physisorption data for gas/solid systems with special reference to the determination of surface area and porosity, Pure Appl. Chem. 57 (1985) 603–619.

[36] J. Huberty, H. Xu, Kinetics study on phase transformation from titania polymorph brookite to rutile, J. Solid State Chem. 181 (2008) 508–514.

[37] A. Di Paola, M. Bellardita, L. Palmisano, Z. Barbieriková, V. Brezová, Influence of crystallinity and OH surface density on the photocatalytic activity of TiO$_2$ powders, J. Photochem. Photobiol. A: Chem. 273 (2014) 59–67.